Performing and Interpreting Experiments Towards Understanding Noise Generation in Displacement Machines

T. Opperwall, A. Vacca

Maha Fluid Power Research Center, Purdue University, West Lafayette, Indiana, USA
E-mail: tjopperwall@gmail.com, avacca@purdue.edu

Abstract

Noise generation in fluid power systems remains an important problem in current applications, and in the expansion of fluid power to new lighter applications such as passenger vehicles. The current research looks to understand noise generation from two main angles, experimental measurements and numerical modeling. This activity shows the experimental procedures and results towards better understanding the noise performance in the particular case of external gear pumps. Sound intensity measurements and analysis of the frequency characteristics of these machines are used to characterize the air-borne noise generated. Better understanding of the key sources and transmission paths of the noise can lead to a better understanding of how to improve the noise performance from a design standpoint. The method of measuring and interpreting the noise performance of several different displacement machines is explained along with the significance of the results pertaining to the design of new quieter hydraulic solutions. This research serves the more general goal as a validation reference for modeling noise generation and propagation from the sources inside the machine and out to the environment.

Keywords: Fluid power, Air-borne noise, Fluid-borne noise, External gear machines

1 Introduction

Positive displacement machines are the prime movers of energy in most fluid power systems. They convert the mechanical energy from an engine or motor shaft into a pressurized fluid which is used in many applications for moving heavy loads. The primary applications of these machines are currently in construction and agriculture equipment, aircraft systems, and heavy industrial equipment.

In typical hydraulic pumps, delivery of fluid is caused by a displacing action of moving mechanical parts. This displacing action is also responsible for generating flow oscillation at the outlet port of the machine and the attached hydraulic lines due to the limitation of a finite number of displacing chambers spread out over each machine cycle. These flow oscillations cause pressure fluctuations when acting against a load, and this is a source of noise in the system called fluid-borne noise (FBN). This FBN propagates through the structure and the system as structure-borne noise (SBN) and then out into the environment as air-borne noise (ABN) as described by Fiebig [1]. Due to the high pressures and forces involved, the sources of FBN and SBN in the displacement machine tend to make them significant sources of noise and vibration in fluid power systems. High noise and vibration is undesirable as it decreases system stability, wastes energy, and reduces comfort of the nearby environment. Even more, the noise and vibration can reduce machine lifetime and introduce more costly maintenance. All of these downsides are present to some degree in most commercial displacement machines, and limit the applications where fluid power systems can be used. In particular, this causes fluid power solutions to be unsuitable to spread to some new applications such as light passenger vehicles.

Previous research has developed advanced models to simulate the physical phenomena in external gear pumps in general such as Vacca and Guidetti [2], Vacca, Dhar, and Opperwall [3], and Dhar and Vacca [4]. In particular, the predictions of these advanced models are used to simulate the noise generation in this type of displacement machine as in Opperwall and Vacca [5].

Many researchers have tried to reduce the radiated noise by minimizing the pressure ripples in the lines of hydraulic systems. This has been done using targeted attenuators such as Helmholtz resonators and expander mufflers demonstrated by Ortwig [6]. Other concepts relating to attenuating line pressure ripple were presented by Earnhart [7]. Edge [8] demonstrated how to take into consideration the system specifications in order to reduce the generated noise. Hartmann [9] optimized an internal gear pump to reduce the FBN. Negrini [10], Lätzel [11], and others have completed work to reduce the noise in external gear pumps through new gear designs. Among others, Ericson,

Johansson, and Palmberg [12] designed optimized axial piston machines.

Bonano [13] compared the frequencies of the SBN to the measured data. Also, Klop and Ivantysynova [14] used sound intensity measurements to match trends between the noise sources and the measured noise for axial piston machines. A similar work was completed by Ngah and Edge [15] using acoustic measurements on components of hydraulic transmissions. Additionally, some work has been done on determining transfer functions and other relationships between noise sources and the radiated ABN such as that done by Pettersson, Weddfelt and Palmberg [16].

The present work seeks to understand the sources and transmission of noise from displacement machines through interpreting measurements of the ABN under a wide range of operating conditions. These measurements were completed in the semi-anechoic chamber at Maha Fluid Power Research Center (Maha).

For the purposes of this research, a reference type of displacement machine is chosen. Four different external gear machines with 38cc/rev displacement were chosen to study the ABN generation. Example gear geometry is shown in Fig. 1. One of the gears is typically driven by an electric motor or combustion engine. This gear then drives the second gear through contact in the meshing zone. Fluid is taken into the volumes of the teeth at the inlet side and carried around the periphery of the machine to the outlet side by the rotation of the gears. The displacing action is achieved by the meshing of the gears where the fluid is forced to move to the outlet port as each tooth volume meshes with the corresponding tooth on the opposite gear. It is this finite number of displacing chambers that causes oscillations in the flow and pressure at the outlet of the pump at frequencies corresponding to the shaft speed and the number of teeth.

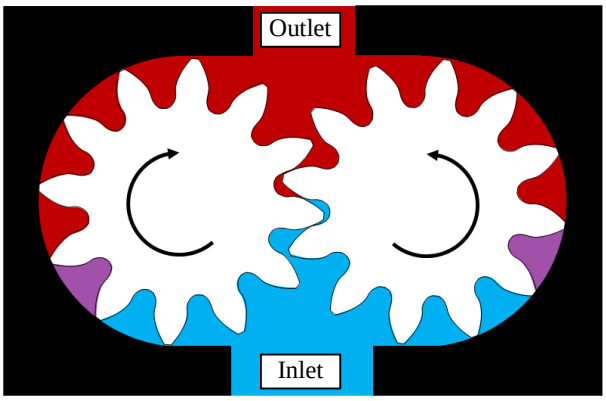

Figure 1: Example geometry and principle of operation of a typical external gear pump.

Three reference pumps of different designs from different manufacturers are compared and are referred to as Pumps 1,2,3. For Pump 2, two different designs are considered, which will further be referred to as Pump 2A and Pump 2B. The noise characteristics of the different pumps will be compared so that additional insight may be gained. The pumps are physically very similar in terms of overall dimensions and features. All three pumps contain pressure compensated lateral plates or bearing blocks. They all feature identical port sizes and shaft couplings/flanges. The pumps are different from each other in a way which is of interest to noise generation. First, Pumps 1 and 3 contain gears with 10 teeth each. Pumps 2A and 2B contain gears with 14 teeth, but with slightly different part geometry that results in a reduced flow ripple generation by pump 2B with respect to Pump 2A. The differing numbers of teeth and the different flow/pressure ripples will result in differing ABN frequency content and magnitudes if the different pumps are compared at the same speed. Finally, Pumps 1, 2A, and 2B share very similar specified operating condition ranges while Pump 3 is limited to a lower pressure range. A description of the measurement techniques and results can be read in the following sections.

2 Methods of Measuring Noise

The first step in the measurement of the ABN is to ensure an accurate measurement technique and calibrated sensors. To complete this, a known sound power source was measured at 62 grid points chosen on a cube of 1.4m by 1.4m by 1m in the semi-anechoic chamber at Maha Fluid Power Research Center of Purdue University (Maha) shown in Fig. 2 and Fig 3.

Figure 2: Semi-anechoic chamber at Maha, from outside the chamber with the doors open.

The semi-anechoic chamber was built to the requirements of ISO 16902-1 [17]. The acoustic insulation is realized by 0.305m acoustic foam wedges attached to walls and ceiling

excluding inside of the measurement frame. The noise floor is 42dB above 150Hz and a reverberation time of 0.11s as reported by Klop [14]. A pump can be mounted to the test rig electric motor, which is isolated from the pump and the chamber by the staggered-stud reflecting wall shown in Fig. 2. An example pump on the test bed is shown in Fig. 3.

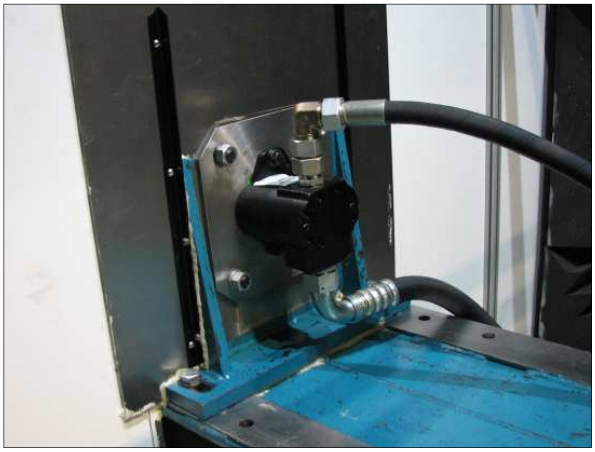

Figure 3: Example pump detail image.

A main use for measurements of ABN in hydraulic systems is through a sound intensity technique for the purpose of calculating total sound power level (SWL). A description of sound intensity calculations can be found in Bendant and Peirsol [18]. This method has previously been applied to fluid power applications by Klop and Ivantysynova [14]. A short summary of the sound power calculations will be included here.

The basis of calculating sound power is measuring the sound intensity at discrete points on a surface surrounding a source. Intensity can be simply stated as the pressure times the velocity in a sound field. As a result, the experiment is completed using at least one pair of microphones along with suitable signal acquisition equipment as shown in Tab. 1. A microphone pair is needed since a means of approximating the velocity field must be used.

Table 1: Description of noise measurement equipment.

Item Type	Description
Sound intensity probe	GRAS, three microphones Type 40A0 – Sensitivity 0.2 dB ref 2·10-5 Pa, ½“ diameter
Pre-amplifier	GRAS, Type 26CB, ¼“ diameter
Signal acquisition module	NI 9234, 4 channels, 51.2 kS/s per-channel maximum sampling rate, ±5 V input
High speed USB Carrier	NI USB 9162 – bus powered carrier for portability

The microphone pairs are spaced at a fixed distance Δr, with one pair separated by 12mm, and a second pair separated by 32mm. Considering a single microphone pair, two separate time signals of pressure are recorded at 50kHz sampling rate for each n discrete point on the measurement grid for N total points.

$$x(t) = x(n\Delta t) \tag{1}$$

$$y(t) = x(n\Delta t) \tag{2}$$

The time signals are divided into segments of 8000 points and zero padded, with 23 total segments for each time signal after the noise sample has been recorded. Each segment is windowed using a Hanning window w(nΔt) which requires a scaling factor of $\sqrt{8/3}$ to account for energy loss due to windowing.

$$w(n\Delta t) = 1 - cos^2\left(\frac{\pi n}{N}\right) \tag{3}$$

The Fast Fourier Transform (FFT) is completed in Matlab on each windowed segment.

$$X_i(k) = \Delta t \cdot \sqrt{8/3} \sum_{n_i=0}^{N_{seg}-1} \left(x_i(n\Delta t) - \bar{x}_i(n\Delta t)\right) \cdot w(n\Delta t) \cdot \exp\left[-\frac{j2\pi kn}{N_{seg}}\right] \tag{4}$$

$$Y_i(k) = \Delta t \cdot \sqrt{8/3} \sum_{n_i=0}^{N_{seg}-1} \left(y_i(n\Delta t) - \bar{y}_i(n\Delta t)\right) \cdot w(n\Delta t) \cdot \exp\left[-\frac{j2\pi kn}{N_{seg}}\right] \tag{5}$$

Finally, the sound intensity average taken across all of the segments and summed over the discrete measurement points can be calculated using the two-sided estimate of the cross-spectral density.

$$I(k) = \frac{Im(\frac{1}{I_{seg}} \cdot \sum_{i=0}^{I_{seg}-1} \frac{2}{N \cdot \Delta t}[X_i^*(k) \cdot Y_i(k)])}{2\pi f(k) \cdot \rho \cdot \Delta r} \tag{6}$$

The total sound power is found by multiplying the calculated sound intensities by the area discrete measurement element. The total sound power level is calculated based on $W_{ref} = 10^{-12}$ Watts.

$$SWL = 10\log_{10}\left(\frac{W}{W_{ref}}\right) dB \tag{7}$$

Once the measurement technique and signal processing algorithm is confirmed, the calibrated sound power source can be replaced by the displacment machine.

A hydraulic test rig circuit was developed for this study as shown in Fig. 4 and Tab. 2. The test rig layout is designed to reproduce the normal open circuit operation of the tested pumps. In particular, a proportional valve is used in closed loop to establish a constant level of pressure at the pump inlet (1 bar), using the hydraulic power supply system present at Maha. Pressure in the inlet lines was measured to examine the pressure fluctuations introduced by the supply and the ripples were found to be in the magnitude of less than 0.2bar, which is within the magnitude of the inlet ripples caused by the pump flow oscillations.

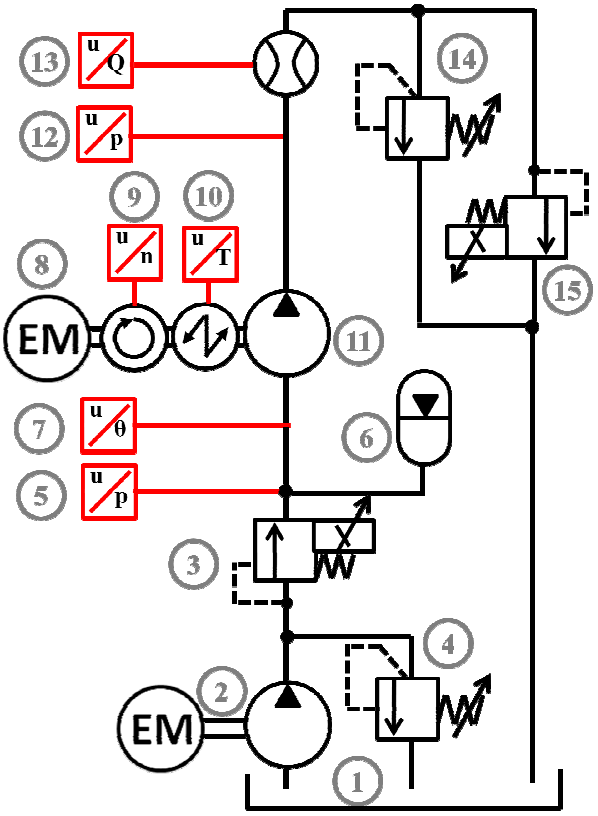

Figure 4: Test rig schematic

Details of the components shown in Fig. 3 are listed in Tab. 2.

Table 2: Details of test rig components.

#	Description	Details
1	Oil Reservoir	Shell Tellus 32 oil, held to 52° C at inlet for 20cSt
2	Maha hydraulic supply	Delivery unit, 80cc/rev, 1185rpm axial piston machine
3	Proportional valve	Hydraforce TS10-26C-8T-N-12DR proportional orifice for pressure reducing to 1bar
4	Pressure relief valve	For setting inlet line pressure from supply pump
5	Inlet pressure sensor	WIKA, 0-100bar, accuracy 0.25% FS
6	Hydraulic accumulator	2 L accumulator to damp inlet, no added precharge
7	Inlet temperature sensor	Omega K-type resistive thermocouple, range 0-120° C, accuracy 1% FS
8	Electric motor	SSB, 500Nm, speed +/-3000rpm
9	Shaft speed sensor	HBM MC60, max 5000rpm, 0.05 Accuracy class
10	Shaft torque sensor	HBM MC60, scale 0-500Nm, 0.05 Accuracy class
11	Test pump	Only feature included inside of noise measurement grid.
12	Line pressure sensor	WIKA, 0-400bar, accuracy 0.25% FS
13	Flow meter	VS 4 by VSE, gear type, 0-400L/min, accuracy 1% FS
14	Pressure relief valve	Safety feature only, set to 300bar.
15	Proportional valve	Hydraforce TS10-26A-8T-N-12DR proportional orifice

3 Sound Pressure and Power Results

The measurement procedure for sound pressure level (SPL) and sound power level (SWL) is similar to that presented by Klop [14]. In order to accurately visualize the sound field generated by the pump, a much finer grid would be required; this may be explored in the future similar to the method of Cho and Bolton [19] in the near field of the pump. An example of the measurement planes for the experimental setup is shown in Fig. 5.

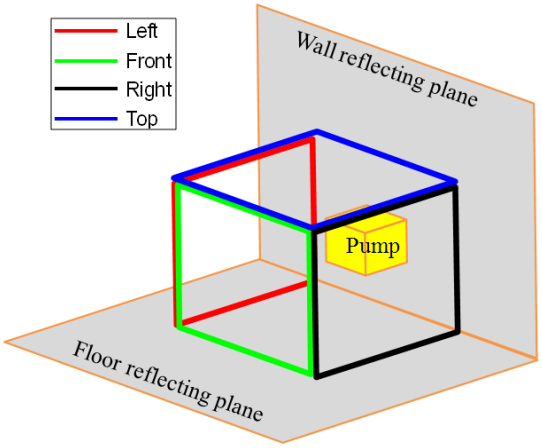

Figure 5: Surfaces for sound measurement.

The measurement volume is a box with six sides. Four of the six sides of the cube are measurement surfaces as shown in Fig. 5. The bottom surface and back surface are reflecting planes of the floor and wall of the chamber respectively. Note that sound pressure level measurements suffer from doubling effects near the main boundaries with the reflecting floor of the chamber. This effect is not seen to a great extent where the top surface meets the reflecting plane since the pump is fixed to the reflecting surface and hence most of the sound is travelling parallel to the surface in that location with little reflection off the surface.

To better understand why noise measurements must be made at many discrete points instead of at just a single point, notice Fig 6. Considering just one discrete point on each of the four measuring surfaces gives insight onto the varying pressure field surrounding the pump. The FFT of the sound pressure is shown in Fig. 6 for one representative point from each of the four measurement surfaces shown in Fig. 5 at an operating condition of 1000rpm with 100bar outlet pressure for Pump 1. The pump primary frequency occurs at 167Hz for Pump 1 based on the shaft speed and the number of chambers. The higher integer multiples are also present.

$$f_1 = \frac{speed * nc}{60} \tag{8}$$

The higher multiples of the pump primary frequency feature can be clearly seen as they dominate the frequency spectrum. Furthermore, while the frequency content occurs in basically the same locations on the spectrum across all four discrete measurement points, it does not contain the same magnitudes at those frequencies. In particular, the left and top sides have generally larger magnitude frequency content at the primary pump frequency and around 1000Hz (the 6th multiple of the primary frequency). The right and front sides have generally smaller magnitude frequency components except the right side is fairly large at the 3rd and 7th multiples of the pump primary frequency.

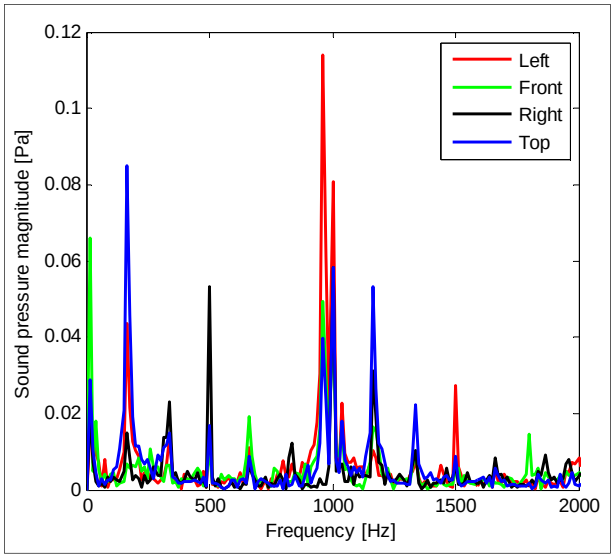

Figure 6: Four points of ABN sound pressure frequency content for Pump 1.

If the sound pressure were to be measured at only a few points, the magnitudes of the various frequency components cannot be considered in terms of absolute value, but only in terms of trends since the set of measurement points is not adequate to calculate an accurate average. Section 4 of this paper will explore the value of other kinds of considerations using fewer discrete points.

The calculated sound intensity map is shown in Fig. 7, along with the total summed SWL. It is shown that the sound intensity also varies over the surface from around 65dB to over 80dB. When these are multiplied by their corresponding areas and summed, the total SWL of 81.49dB is calculated.

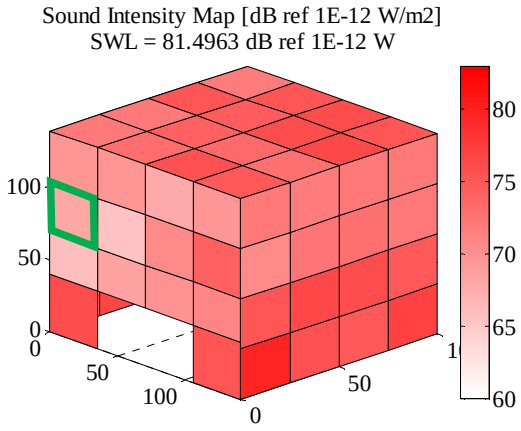

Figure 7: Example sound intensity map with representative point highlighted.

Total SWL measurements for all four pumps is shown in Fig. 8. Each data point in Fig. 8 represents the sum of a set of 62 noise measurements taken over the measurement grid. Total SWL measurements were completed for the operating

ranges of 1000rpm to 2500rpm and 50bar outlet pressure to 250bar outlet pressure except for Pump 3 where its specifications limited it to 200bar. An interesting feature of the pumps is shown in Fig. 8. The pump which is designed to operate at a lower operating condition produces the lowest SWL at 1000rpm across all three measured pressures.

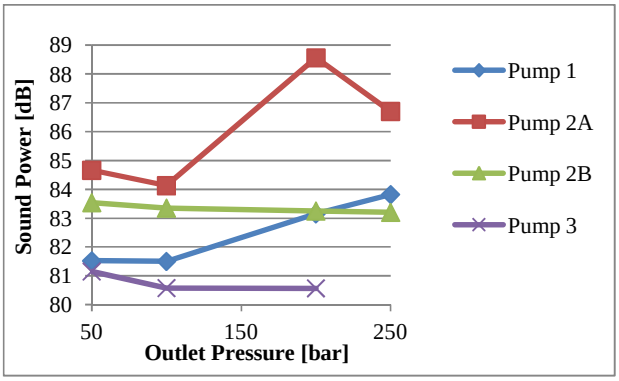

Figure 8: Total SWL for 1000rpm operating speed.

This result shows that the while the original Pump 2A was the noisiest at 1000rpm, Pump 2B achieved a reduction in SWL across the pressure range which brought it into line with Pumps 1 and 3. The improvement in Pump 2B can be fully attributed to the reduced pressure ripple generation. It has been shown by other authors as well, as in the modeling work done in parallel with this project, that the frequencies of the FBN can be predicted or measured via various approaches such as in Vacca and Guidetti [2]. It is also shown and can be perceived in the experimental tests that the main frequencies of the ABN are mainly the same frequencies as present in the FBN area inside the outlet volume of the pump and the attached hydraulic lines. According to that understanding along with the experimental results shown in Fig. 8, the conclusion can be made that the reduction in FBN can have a large positive effect on the ABN. Furthermore, the main difference in SWL between various commercial pump products can likely be attributed to how well the pump design handles the generation of FBN.

4 Representative Point Measurements

The noise measurements completed in the previous section involved holding the pump to a steady-state condition while manually moving the sound probe to 62 distinct locations on the microphone grid. The advantage of this method is that the total sound power of the pump can be accurately measured without an impact of the structures and equipment outside of the grid volume. Also, this results in a much higher accuracy estimation of the total sound power of the pump, which can be used to compare various difference pumps on a level playing field without the interference from other sources. The main disadvantage to the SWL method over the discrete grid is the time required for each operating condition. This leads to a very coarse grid of operating points which is not good for spotting trends related to small changes in speed or pressure. In order to make comparisons at a finer set of operating points, a single representative point highlighted in Fig. 7 is chosen. This point was selected as it reflects the average value of sound pressure level at many speeds across all of the different combinations of pumps and operating conditions tested for SWL. The magnitudes of the sound pressure measured at the reference point cannot be reliably used for characterizing specific features about the total noise generated by the pump, but the frequency content can be analyzed on a much finer set of operating points in order to spot trends or features in the frequency domain.

First, at a single speed and pressure of 1000rpm and 100bar, the FFT of the sound pressure can be analyzed comparing all four pumps simultaneously as shown in Fig. 9. This comparison shows several interesting features of the different pump operations. The frequency range is limited to 1200Hz in order to highlight the differences between the various pumps in this range. First, the primary pump frequencies can be interpreted from this graph. Additionally, the number of teeth on the gears in each pump can be inferred as long as the speed is known, or vice versa. From this graph (and confirmed by the pump catalog specifications) it can be stated that the primary pump frequency corresponding to Pump 1 and Pump 3 is 167Hz as was previously stated in Fig. 6. This corresponds to a 10 tooth pump at 1000rpm. Likewise, for Pumps 2A and 2B, the primary pump frequency is 233Hz which corresponds to a 14 tooth pump at 1000rpm. Looking closer at the FFT in Fig. 9, the frequencies shown for Pumps 1 and 3 correspond very closely to each other despite being different designs from different manufacturers. This occurs mainly because the main features relating to noise generation are very similar. Namely, the number of teeth, the relative size of the pump, and the pressure compensated design. The close SWL results in Fig. 8 also suggests the different designs are operating in a very similar manner. Similarly, the FFT results at the representative point for Pumps 2A and 2B are very similar, with a small decrease in the overall magnitude seen for Pump 2B with respect to Pump 2A.

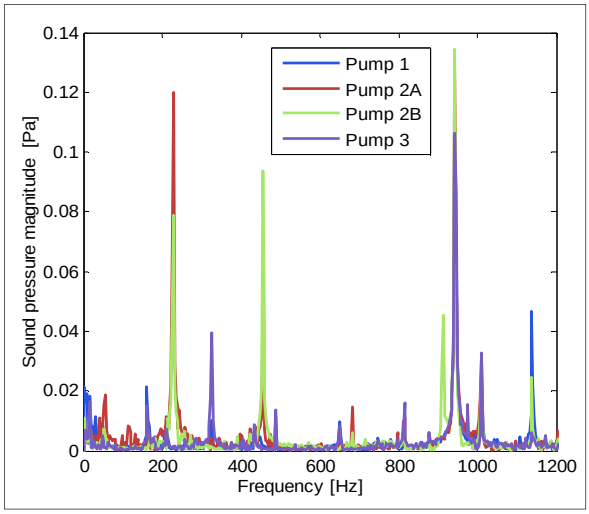

Figure 9: ABN at representative point for all pumps

The peak at 1000Hz for all four pumps see in Fig. 9 indicates that the structure, the system, or features of the geometry of the measurement location are contributing to the sound pressure frequency content. A peak at 1000Hz would be expected for the 10 tooth pumps as that corresponds closely with the sixth multiple of the pump primary frequency. However, a peak at 1000Hz would not be expected based on the FBN of Pumps 2A and 2B since the nearest multiples of the primary pump frequencies are at the 4^{th} multiple at 933Hz, and the 5^{th} multiple at 1167Hz. However, at 1000Hz, all four pumps have a strong peak in frequency. The ability to detect these kinds of features is simultaneously one of the best things and one of the most difficult things about these kinds of measurement comparisons.

In order to better understand what is happening in the frequency domain, a wider range of frequencies and operating conditions must be considered. The method for this study selected was to hold the outlet pressure constant at 50bar while adjusting the speed across the operating range and recording the sound pressure at the representative measurement point shown in Fig. 7. This results in a fine definition of the pressure spectra across a wide range of operating conditions. The results for Pump 1 are shown in Fig. 10.

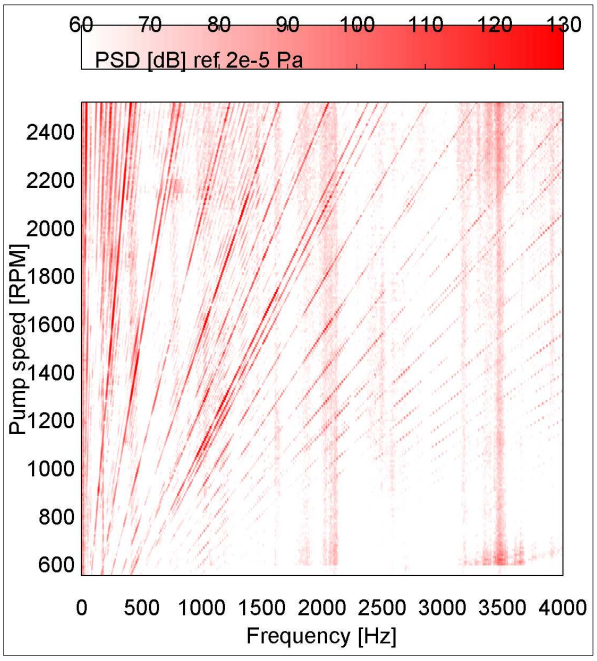

Figure 10: Representative point power spectral density for Pump 1 at 50bar outlet pressure.

The angled lines in Fig. 10 are created by the relationship between the pump speed and the primary pump frequency. The slope of each line is determined by the integer multiples of the pump speed times the number of teeth divided by sixty as shown in Eqn. 8. Figure 10 in particular highlights the fact that the vast majority of the energy in the sound pressure is centered at the multiples of the primary pump frequency. Additional energy content is shown at the shaft frequency represented by the farthest left line in Fig. 10. System/structural frequencies can also be seen in the image represented by vertical lines; that is, frequency content that is independent of the pump speed and present for all of the displayed operating conditions. Also to be noted is that the frequencies with the most power all occur at relatively low frequencies under about 2000Hz.

An alternate way of looking at the information is to take the integral at each pump speed and sum from left to right while displaying the total value of the PSD. For Pump 1, this alternate display is shown in Fig. 11. This method of looking at it allows for the different noise results to be considered in terms of their contribution to the overall PSD. The frequency range here is cut to 2000Hz since the integral sum was nearly constant after that point for all speeds. Of particular interest to understanding the generation of noise in displacement machines is looking at the dominating frequencies at each speed. In particular, in the speed range of 1000rpm to 1800rpm, the PSD of the ABN is dominated by the same frequencies that are present in the FBN.

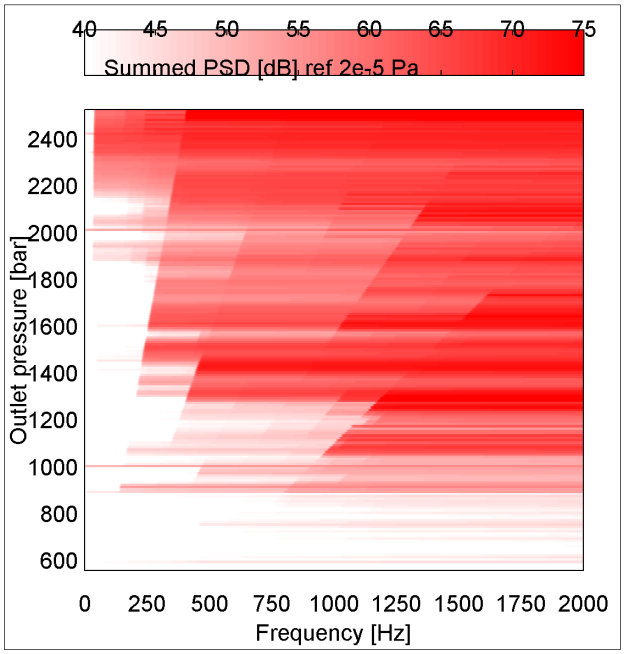

Figure 11: Summed PSD of representative point measurements for pump 1 at 50bar outlet pressure.

Figure 13 shows the same PSD map for Pump 2B. It can be said that there is remarkable similarity between Figs 10 and 11. Everything that was said about Fig. 10 can thus be repeated for Fig. 12.

Of interest after comparing both results in Figs. 10 and 12 together is that the same system/structural frequency features are present in both images, in particular at about 2000Hz and 3500Hz.

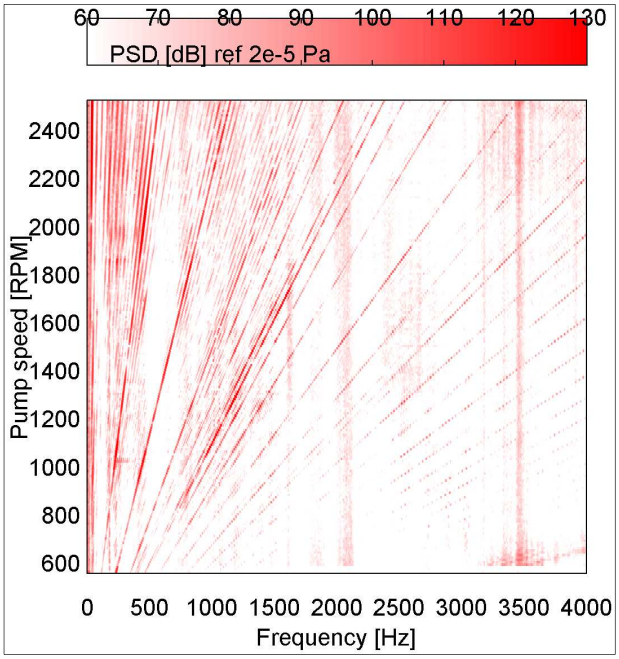

Figure 12: Representative point power spectral density for Pump 2B at 50bar outlet pressure.

For further comparison and completeness, the summed PSD for Pump 2B is shown in Fig. 14.

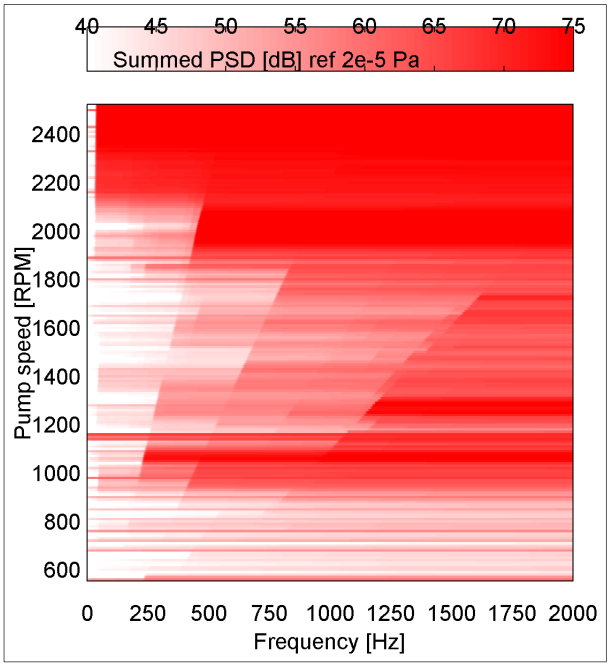

Figure 13: Summed PSD of representative point measurements for pump 2B at 50bar outlet pressure.

The results for Pumps 2A and 3 were omitted as the similarities to the already presented data were very strong.

A final result of the representative point measurements is to compare the average sound pressure level of all four pumps across the same speed range. This result is shown in Fig. 15.

This once again shows the remarkable similarity in the results for all four of the pumps. In particular, the peaks around 1000rpm and 1250rpm in the SPL. This demonstrates a possible bias in all of the measurements. The shape of this function across all four pumps is very nice to describe both the influence that the acoustic environment has on the sound pressure, and also the similarity in the performance of the different models of external gear pump.

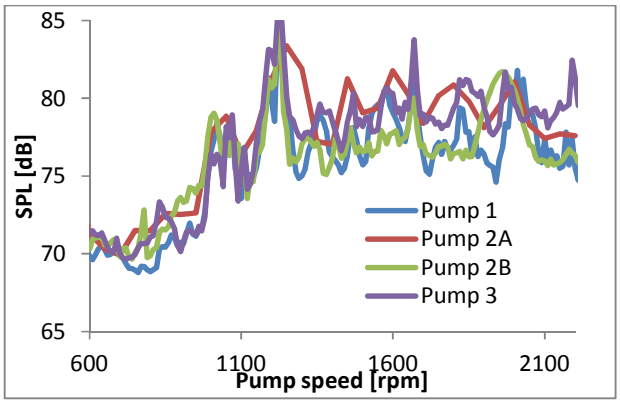

Figure 14: Representative point SPL at 50bar outlet pressure.

5 Conclusions

From the experimental results for total sound power, the total ABN generated by each pump can be measured. The frequency spectra for the representative point measurements for Pumps 1 and 2B shown in Figs. 10-14 demonstrate that for the region of 1000rpm through 1800rpm, the dominating frequencies in the ABN match the main frequencies in the FBN. Thus, since the dominating effect in that speed range can be declared to be the FBN. The lower pressure ripple Pump 2B should be expected to have an improvement in the radiated noise in this range over its counterpart Pump 2A, and this expectation was confirmed. The representative point measurements are very helpful in understanding the important features in the ABN, and can be used to aim further design improvements. Also, the procedure is general and can be completed for different pumps. For very similar styles of pump (all are 38cc/rev external gear pumps), the results of these experiments show clues to the most important sources of FBN and SBN in different speed ranges. Optimal speed ranges could also be measured or designed for based on the measurement data. Additionally, the human factor should be taken into account when considering design changes to the effect that decreasing the magnitude of the primary pump frequency in the FBN with no regard for the higher frequency noise may result in a pump that is perceived to be noisier, instead of quieter, despite a lower total sound power. All of the sound power measurements and representative point measurements shown previously in this work are good for understanding important components in the ABN, but future work will be done to better apply how humans in contact with these systems will actually be affected by changes to the pump performance.

As better understanding of the effect of FBN on ABN is gained, the possibility of using an experimental approach in combination with the design process could lead to new methods of designing better displacement machines. The main future work of these experiments is closing the loop and reconciling measured noise with the fluid dynamic model of the pump and developing coupled acoustic model.

Nomenclature

Designation	Denotation	Unit
FBN	Fluid-borne noise	
SBN	Structure-borne noise	
ABN	Air-borne noise	
$x(t)$	Sound pressure signal 1	[Pa]
$y(t)$	Sound pressure signal 2	[Pa]
n	Number for current measurement	
N	Total number of points	
$X_{\mathrm{i}}(k)$	FFT for sound pressure signal 1	[Pa]
$Y_{\mathrm{i}}(k)$	FFT for sound pressure signal 2	[Pa]
N_{seg}	Number of points in each segment	
$I(k)$	Sound intensity	[W/m^2]
$f(k)$	Frequency range	[Hz]
ρ	Density of air	[kg/m^3]
Δr	Distance between mics	[m]
f_1	First pump frequency feature	[Hz]
nc	Number of chambers in pump	

References

[1] Fiebig, W., 2007, "Location of Noise Sources in Fluid Power Machines," International Journal of Occupational Safety and Ergonomics, 13 (4), 441-450.

[2] Vacca A., Guidetti M., 2011, Modeling and Experimental Validation of External Spur Gear Machines for Fluid Power Applications, Elsevier Simulation Modeling Practice and Theory, 19 (2011) 2007–2031.

[3] Vacca A., Dhar S., Opperwall T., 2011, A Coupled Lumped Parameter and CFD Approach for Modeling External Gear Machines, SICFP2011 The Twelfth Scandinavian International Conference on Fluid Power, May 18-20, 2011, Tampere, Finland.

[4] Dhar S., Vacca A., 2012, A Novel CFD- Axial Motion Coupled Model for the Axial Balance of Lateral Bushings in External Gear Machines, Elsevier Simulation and Modeling Practice and Theory. 2012; 26: 60-76.

[5] Opperwall T., Vacca A., "A combined FEM/BEM model and experimental investigation into the effects of fluid-borne noise sources on the air-borne noise generated by hydraulic pumps and motors." Proceedings of the Institution of Mechanical Engineers, Part C: Journal of Mechanical Engineering Science, First published online on April 22, 2013. (Print publication pending)

[6] Ortwig, H., 2005, "Experimental and Analytical Vibration Analysis in Fluid Power Systems," International Journal of Solids and Structures, 42, 5821-5830.

[7] Earnhart, N., Marek, K., and Cunefare, K. Novel, compact devices for reducing fluid-borne noise. in SAE 2011 Noise and Vibration Conference and Exhibition. 2011. Grand Rapids, MI.

[8] Edge, K. A., 1999, "Designing Quieter Hydraulic Systems – Some Recent Developments and Contributions," Proceedings of the Fourth JHPS International Symposium on Fluid Power, Tokyo, Japan, 3-27.

[9] Hartmann K., Harms H.H, Lang T. 2012 A Model Based Approach to Optimize the Noise Harmonics of Internal Gear Pumps by Reducing the Pressure Pulsation, 8th International Fluid Power Conference (IFK), March 26-28, 2012, Dresden, Germany.

[10] Negrini, S. "A Gear Pump Designed for Noise Abatement and Flow Ripple Reduction" International Fluid Power Exposition and Technical Conference. 23-25 April 1996.

[11] Lätzel, M. Schwuchow, D., "An innovative external gear pump for low noise applications" 8th International Fluid Power Conference (IFK), March 26-28, 2012

[12] Ericson L, Johansson A and Palmberg J-O. Noise reduction by means of non-uniform placement of pistons in fluid power machines. In: Proceedings of the 2009 ASME dynamic systems and control conference and bath/ASME symposium on fluid power & motion control theme: system engineering, Hollywood, CA, USA, 12–14 October 2009.

[13] Bonanno, A., and Pedrielli, F., 2008, "A Study of the Structure borne Noise of Hydraulic Gear Pumps," 7th JFPS International Symposium on Fluid Power, 641-646.

[14] Klop, R. and Ivantysynova, M. 2010. Sound Intensity Measurements to Investigate Noise Generation of Hydrostatic Transmissions Proceedings of the 7th

International Fluid Power Conference Aachen 2010 (7IFK), Vol. 2, 229-242

[15] Ngah, Z. and Edge, K.A., "The measurement of positive displacement pump and motor noise using sound intensity techniques." Off-highway Powerplant Congress and Exposition, SAE, Warrendale, USA, pp. 1-6, September, 2001

[16] Pettersson, M., Weddfelt, K., and Palmberg, J.-O., "Prediction of structural and audible noise from axial piston pumps using transfer functions." In Proc. Of Eighth Bath International Fluid Power Workshop, 1995

[17] ISO 16902-1:2003 Hydraulic fluid power -- Test code for the determination of sound power levels of pumps using sound intensity techniques: Engineering method -- Part 1: Pumps, 2003.

[18] Bendant J.S. and Peirsol, A.G., "Random Data – Analysis and Measurement Procedures." John Wiley & Sons, INC, ISBN 0-471-31733-0, 2000

[19] Cho, Y. T., and Bolton, J. S., 2004, "Acoustical Visualization of a Refrigeration Compressor by using Statistically Optimized Nearfield Acoustical Holography in Cylindrical Coordinates," NOISE-CON, 175-182.